

ATIVIDADE VESPERTINA DO DIA 30-03-2012 DURANTE A CONVENÇÃO ANUAL AIUM – AMERICAN INSTITUTE OF ULTRASOUND IN MEDICINE

CURSO DE ATUALIZAÇÃO - SHEAR WAVE IMAGING (IMAGENS DAS ONDAS DE CISALHAMENTO)

Moderadores: Thomas Szabo, PhD e Tomy Varghese, PhD

Esta sessão teve o propósito de atualizar sobre os avanços clínicos e tecnológicos das imagens através das shear waves (ondas de cisalhamento).

1. Primeira palestra : ONDA DE CISALHAMENTO SONDANDO A ESTRUTURA TECIDUAL E SUAS ALTERAÇÕES, ministrada por Armen Sarvazyan, PhD

O número de trabalhos científicos que utilizam a onda de cisalhamento ultrassônica cresceu enormemente na última década. E novas técnicas foram propostas para avaliar e detectar as anormalidades teciduais, por meio da compressão e geração de ondas de elásticas. Inicialmente os sistemas de imagem elastográfica geravam ondas compressivas nos tecidos por vibradores externos. No final de 1990, vários laboratórios iniciaram o desenvolvimento de um método alternativo para gerar ondas de cisalhamento nos tecidos através da força de radiação acústica. As ondas tensionais de cisalhamento induzidas remotamente pela força de radiação acústica de ultrassom focado pode ser muito bem localizada, permitindo um posicionamento preciso do local de excitação e oferece ao médico um dedo virtual para testar as regiões internas de interesse. As velocidades das ondas de cisalhamento variam de 1 a 100m/s, ou seja, essa grande escala de frequências permite maior gama de utilização:

- com as frequências mais baixas a penetração é maior;
- com as frequências mais elevadas a penetração é menor devido ao aumento da atenuação. De uma forma geral as ondas de cisalhamento são muito atenuantes e são utilizados geradores remotos dessas ondas por meio da força de radiação acústica.

Foi demonstrado que uma sonda focada de US com intensidades e exposições similares àquelas do US diagnóstico podem induzir uma força de radiação grosseira da ordem de 0.01 a 0.1N/cm² e o deslocamento da onda de cisalhamento dos tecidos de partes moles é da ordem de 10µm ou mais, o que pode ser facilmente detectado pela US e RNM. Devido à elevada atenuação das ondas de cisalhamento é possível induzir oscilações mecânicas dentro de uma área dos tecidos, nas proximidades de um ponto específico, por meio de um feixe US focalizado. De tal forma que a velocidade de propagação da onda de cisalhamento dos tecidos dependerá principalmente das propriedades teciduais e não das condições das interfaces. A tecnologia US existente e os dispositivos que ela utiliza podem ser rapidamente para esses propósitos, eliminando a necessidade de desenvolvimento de uma tecnologia distinta. Ele citou dois trabalhos, mas só localizamos 1 deles:

1. [Ultrasound Med Biol.](#) 1998 Nov;24(9):1419-35. **Shear wave elasticity imaging: a new ultrasonic technology of medical diagnostics.** [Sarvazyan AP](#), [Rudenko OV](#), [Swanson SD](#), [Fowlkes JB](#), [Emelianov SY](#).

Abstract

Shear wave elasticity imaging (SWEI) is a new approach to imaging and characterizing tissue structures based on the use of shear acoustic waves remotely induced by the radiation force of a focused ultrasonic beam. SWEI provides the physician with a virtual "finger" to probe the elasticity of the internal regions of the body. In SWEI, compared to other approaches in elasticity imaging, the induced strain in the tissue can be highly localized, because the remotely induced shear waves are attenuated fully within a very

limited area of tissue in the vicinity of the focal point of a focused ultrasound beam. SWEI may add a new quality to conventional ultrasonic imaging or magnetic resonance imaging. Adding shear elasticity data ("palpation information") by superimposing color-coded elasticity data over ultrasonic or magnetic resonance images may enable better differentiation of tissues and further enhance diagnosis. This article presents a physical and mathematical basis of SWEI with some experimental results of pilot studies proving feasibility of this new ultrasonic technology. A theoretical model of shear oscillations in soft biological tissue remotely induced by the radiation force of focused ultrasound is described. Experimental studies based on optical and magnetic resonance imaging detection of these shear waves are presented. Recorded spatial and temporal profiles of propagating shear waves fully confirm the results of mathematical modeling. Finally, the safety of the SWEI method is discussed, and it is shown that typical ultrasonic exposure of SWEI is significantly below the threshold of damaging effects of focused ultrasound

Conclusão: nas últimas 2 décadas, o uso das ondas de cisalhamento na avaliação da elasticidade em medicina tornou-se um dos tópicos mais "quentes" do diagnóstico médico.

2. **Segunda palestra : NOVOS IMPULSOS TORNAM COMPLEXAS AS ONDAS DE CISALHAMENTO PARA AS IMAGENS ELASTOGRÁFICAS**, ministrada por James Greenleaf, bioengenheiro da Mayo Clinic

A propagação das ondas de cisalhamento dos tecidos pode ser medida com:

- Equipamento Doppler com alta frequência de pulso
- métodos de correlação
- métodos que utilizam o formador de feixe padrão.

Para se conhecer as propriedades do material ou tecido analisado pela elastografia, que exigem medida das características de propagação das ondas de cisalhamento, tais como velocidade vs frequência, são empregados módulos complexos de viscoelasticidade utilizando modelos físicos apropriados que usam a geometria e as propriedades dos tecidos .

O autor demonstrou durante a aula modelos que testavam o efeito da geometria tecidual sobre as ondas de cisalhamento, outros onde se utilizavam pulsos focalizados em Phantoms de gelatina, modelos com impulsos supersônicos ou que podem atingir grandes profundidades e outros modelos com feixes em pico que apresentavam ondas de cisalhamento em todos os pontos, testados a uma profundidade de 20mm. O problema oposto a este é caracterizado pelo cálculo de módulos de armazenamento e perda em função da frequência, os quais requerem movimentação tecidual apropriada, que por sua vez requerem uma elevada relação entre sinal/ruído da distribuição da força de radiação dinâmica. Esta nova distribuição da força de radiação, a qual promove realce da movimentação tecidual por meio das medidas ultrassonográficas dessa movimentação, permite a solução do problema inverso representado pelas propriedades do material tecidual. O autor conclui que o feixe supersônico é melhor para profundidade enquanto que o pulso em pico tem maior liberdade e é, portanto, mais flexível.

3. **terceira palestra : FORÇA DE RADIAÇÃO ACÚSTICA- IMAGEM DE ELASTICIDADE BASEADA NA ONDA DE CISALHAMENTO CARACTERIZANDO QUANTITATIVAMENTE A DUREZA DOS TECIDOS DE PARTES MOLES** , ministrada por Mark Palmeri, bioengenheira da universidade de Duke – NC

A modalidade de imagem que avalia a elasticidade pelas ondas de cisalhamento tem sido foco de pesquisa por vários anos para caracterizar de forma não invasiva a dureza dos tecidos de partes moles e diagnosticar doenças, monitorar longitudinalmente a progressão da doença e estabelecer a conduta de procedimentos invasivos. A força de radiação acústica ultrassônica, baseada nas imagens das ondas de cisalhamento, foram recentemente transportadas para a prática clínica e a disponibilização comercial dessa tecnologia recém adquirida tem conduzido para novas aplicações clínicas. Foi mostrada várias características técnicas dos novos equipamentos, tais como a implementação das imagens que utilizam ondas de cisalhamento por meio da excitação da força de radiação acústica transitória focalizada. Considerações sobre as configurações da excitação focalizada, estimativas do

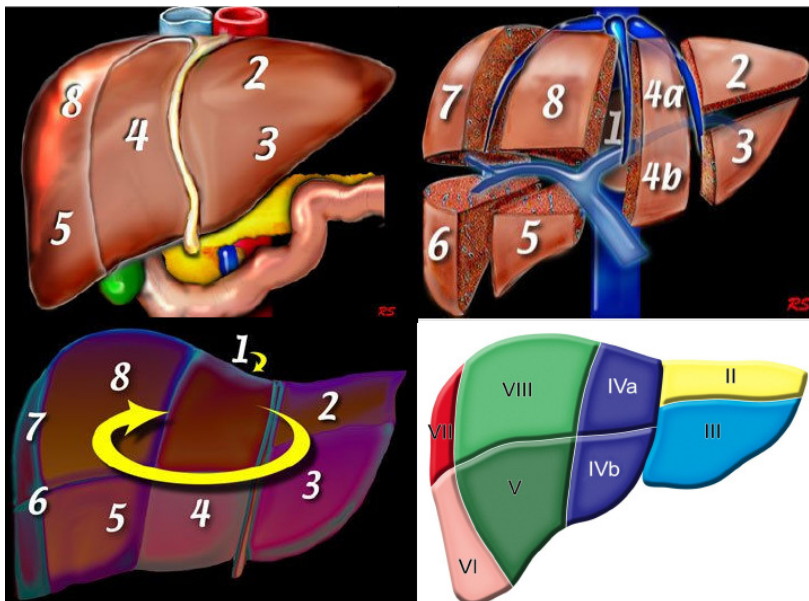
deslocamento e algoritmo das velocidades de propagação da onda de cisalhamento. Foi revista as estimativas dos diferentes tempos de chegada das ondas de cisalhamento em função:

- de um artefato introduzido para gerar um baixo deslocamento do sinal/ruído,
- da movimentação do paciente/médico durante a obtenção da imagem
- da reflexão da onda de cisalhamento em função das interfaces e características das estruturas anatômicas.

Foram apresentadas as aplicações clínicas das imagens que utilizam as ondas de cisalhamento para estimar a elasticidade dos tecidos com foco primário no estadiamento da fibrose hepática resultante de várias etiologias distintas.



Imagens da Dra Eloiza Quintela, Grupo de Hepatites Virais – IIER, SP



Imagens da Dra Eloiza Quintela, Grupo de Hepatites Virais – IIER, SP

Sabe-se que o fígado esteatótico pode ser decorrente de síndrome metabólica ou da esteatose simples e pode progredir para esteatopatite, cirrose e carcinoma hepatocelular nos casos mais graves. Embora a biópsia hepática seja considerada o padrão ouro, ela é muito invasiva, tem custo elevado, envolve riscos para o paciente e não é adequada para análise evolutiva (progressão ou regressão da doença).

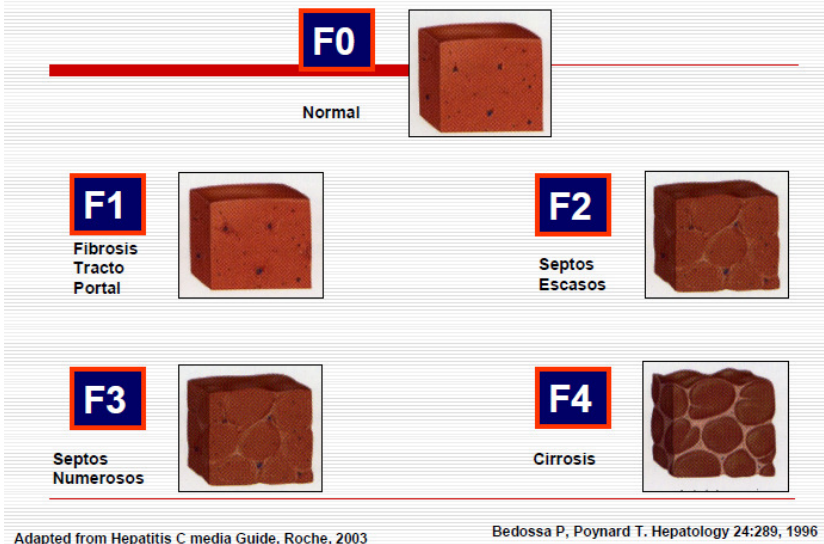
Hepatite C: Diagnóstico Histopatológico Biópsia Hepática Percutânea



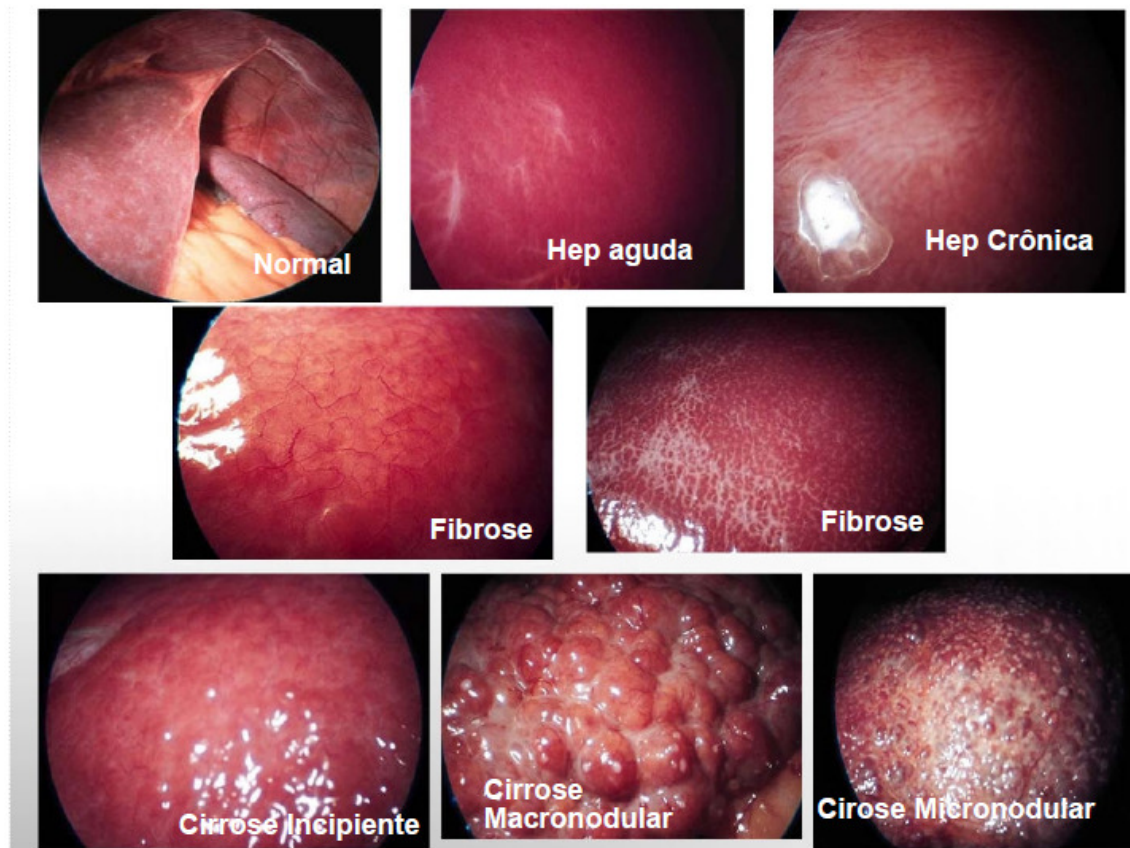
Imagens da Dra Eloiza Quintela, Grupo de Hepatites Virais – IIER, SP

Foram estudados um total de 172 pacientes em Duke University de março de 2008 a 2010, todos acima de 18 anos, sem sinais de doenças hepáticas co-existentes, sendo 65 homens e 107 mulheres. A fibrose foi classificada em 5 estágios, de acordo com a classificação Metavir em 0, 1, 2, 3 e 4:

Biopsia: Clasificación METAVIR para Fibrosis



Imagens da Dra Eloiza Quintela, Grupo de Hepatites Virais – IIER, SP



Imagens da Dra Eloiza Quintela, Grupo de Hepatites Virais – IIER, SP

Para estadiamento foi utilizado o equipamento Siemens Sonoline Aantaris com sonda de 2MHz para a força ARFI e 4MHz para o feixe rastreador. Foram sempre obtidos três valores em cada local do fígado e os resultados demonstraram 90% de sensibilidade, 90% de especificidade, para diferenciar entre os estágios F0 – F2 e F3 – F4 e foi estabelecido 4.24KPa como valor de corte. Não houve correlação entre o peso corporal e grau de fibrose hepática, mas vários pacientes obesos não puderam ser examinados: 10% (obeso discreto), 20% (obesos moderados) e 58% (obesos severos). Mas outros fatores podem estar afetando a elasticidade hepática, tal como a pressão hepática intersticial. Atualmente estão utilizando o equipamento AS2000 (siemnes) acoplado a um equipamento tridimensional que permite a aquisição das imagens das onas de cisalhamento em 3F, o que permite maior precisão em meios não homogêneos.

Conclusão:

a elastografia que utiliza ondas de cisalhamento tem grande precisão para avaliar a presença de fibrose em meios não homogêneos, mas precisa melhorar a penetração para avaliar os pacientes com elevado peso corporal.

4. **quarta palestra : IMAGEM DE ELASTICIDADE BASEADA NA ONDA DE CISALHAMENTO – UMA PERSPECTIVA CLÍNICA**, ministrada pelo Dr. David Cosgrove, ciências da imagem Imperial College, London

As vantagens da imagem de elasticidade ARFI (força de radiação acústica) - baseada na onda de cisalhamento são:

- o impulso compressivo é criado dentro do paciente;
- é capaz de formar uma imagem;
- é capaz de quantificar em metros por segundo.

O FIBROSCAN é um equipamento que utiliza a elasticidade transitória e é muito aceito pelos hepatologistas na Europa mas atualmente existe uma versão mais avançada produzida pela Siemens, que utiliza a imagem de elasticidade ARFI. Outro equipamento, o AIXPLOREER foi utilizado para estruturas superficiais e atualmente está sendo utilizado para órgãos abdominais. É rápido e poderá ser usado em 3D. Aas máquinas que utilizam as propriedades das ondas de cisalhamento medem a velocidade e esse valor pode ser convertido em kPA, mas esta conversão pode induzir a erros, pois não necessariamente a velocidade reflete a dureza tecidual. Por exemplo: os cistos não suportam as ondas de cisalhamento, embora sejam estruturas moles. Atualmente está sendo realizado um estudo multicêntrico europeu com **1800 pacientes que avaliará a elastografia em nódulos mamários** quanto a reprodutibilidade, risco de malignidade e capacidade de redução das biópsias desnecessárias. Em 758 massas já analisadas, observou-se:

- que a variabilidade intra observador é mínima, sendo quase perfeito nesse quesito (ICC ≥ 0.94);
- mas a variabilidade inter observador é moderada (K=0.76);
- permitiu mudar a classificação BIRADS em alguns pacientes realizando um upgrade do BIRADS 3 e um downgrade do 4^a, aumentando a especificidade de 61.1% para 78.5% (p<0.0001). a acurácia aumentou para 0.962

O Aixplores SWE foi avaliado em **146 nódulos tireoidianos, sendo 29 cânceres**, e quando houve associação da elastografia com a US, aumentou a precisão para a caracterização da lesão maligna e citou a referência:

Shear Wave Elastography: A New Ultrasound Imaging Mode for the Differential Diagnosis of Benign and Malignant Thyroid Nodules

F. Sebag, J. Vaillant-Lombard, J. Berbis, V. Griset, J. F. Henry, P. Petit and C. Oliver

Abstract

Context: Elastography uses ultrasound (US) to assess elasticity. Shear wave elastography (SWE) is a new technique that estimates tissue stiffness in real time and is quantitative and user independent.

Objectives: The aim of the study was to assess the efficiency of SWE in predicting malignancy and to compare SWE with US.

Design: Ninety-three patients and 39 control subjects were included in the study. Predictive value of SWE was assessed by correlation between elasticity, US parameters, and histology. Elasticity index (EI) was first analyzed alone. Scores have been constructed with echographic parameters, *i.e.* vascularity, hypoechogenicity, and microcalcifications (Score 1 = US Score), and with the same parameters plus EI (Score 2 = US+SWE Score). For statistical analysis, univariate and multivariate analysis and receiver operating characteristic curves were used.

Results: A total of 146 nodules from 93 patients were analyzed. Twenty-nine nodules (19.9%) were malignant. Mean (\pm SD) EI was 150 ± 95 kPa (range, 30–356) in malignant nodules vs. 36 ± 30 (range, 0–200) kPa in benign nodules ($P < 0.001$, Student's *t* test). For a positive predictive value of at least 80%, characteristics of tissue elasticity (cutoff, 65 kPa) were: sensitivity = 85.2%, and specificity = 93.9%. Characteristics of the US Score were: sensitivity = 51.9% [95% confidence interval (CI), 33.1; 70.7], and specificity = 97% (95% CI, 93.6; 1). Characteristics of the US+SWE Score were: sensitivity = 81.5% (95% CI, 66.9; 96.1), and specificity = 97.0% (95% CI, 93.6; 1).

Conclusion: Promising results have been obtained with SWE. This technique may be applied to multinodular goiters. Larger prospective studies are needed to confirm these results and to define the respective places of SWE, US, and FNA.

Palpable thyroid nodules are very common, with an estimated prevalence that ranges between 5.3% in women and 0.8% in men in the Whickham survey (1). Additionally, up to 68% of the general population has thyroid nodules, even when the thyroid gland is normal to palpation (2). The

prevalence of such infracentimetric nodules discovered by ultrasonography increases with age (2, 3). The majority of thyroid nodules are benign (colloid nodule, follicular adenoma, cyst, and thyroiditis), but 5 to 15% are malignant (papillary, follicular, medullary, or anaplastic carcinoma) (2).

After clinical examination, thyroid ultrasound (US) is used as a first-line procedure to help differentiate benign and malignant nodules. Several US features have been associated with malignancy: microcalcifications, hypoechogenicity, intranodular vascularity, irregular margins, and absent halo sign (4). All of these features alone are poorly predictive of malignancy. In combination, their specificity increases, but sensitivity decreases (5). After clinical examination and thyroid US, fine-needle aspiration (FNA) biopsy has a central role in differentiating benign from malignant thyroid lesions. In expert centers, FNA provides useful results in 65–75% of examined nodules (6). Approximately 60–70% of aspirates prove to be cytologically benign, 5% are positive for papillary carcinoma, and 5–15% remain inconclusive. The remaining 15–25% of aspirates are indeterminate or suspicious (7). The latter two results offer a challenging dilemma for the clinician. Indeed, FNA is limited by sampling difficulties with inadequate collected specimens and by overlap in morphological signs between benignity and malignancy. When FNA results are indeterminate or suspicious, most clinicians recommend surgical excision. Then, the sensitivity of FNA will increase, whereas its specificity will decrease (8). The poor quality of FNA specimens may be the source of diagnostic errors with false-negative and false-positive results that reached 25 and 9.9%, respectively, in a recent multiinstitutional survey (9).

Therefore, there is a need for another way to evaluate thyroid nodules. Over the last few years, a new diagnostic tool has emerged that uses US to assess tissue elasticity and stiffness to differentiate malignant from benign lesions. Stiffness is usually correlated with malignancy because benign lesions are supposed to be softer (10). Different techniques of elastography have been applied to thyroid nodules, based on real-time elastography and off-line processing of strain images (11, 12, 13), external compression (14, 15, 16), or carotid artery vibrations (17). However, the widespread applicability of these techniques is limited because they cannot be used in the evaluation of multinodular goiters, which represent about 40% of nodular thyroid glands (18). There is no consensus about the risk of cancer per patient, regardless of whether one or multiple nodules are present. Indeed, the prevalence of carcinoma was found to be lower in patients with a solitary nodule than in patients with multinodular thyroid (19, 20), but the prevalence was equal in another study (21). More recently, a technique has been developed that uses tracking of shear wave propagation through tissue to obtain the elastic modulus (22). This new shear wave elastography (SWE) is operator-independent, reproducible, and quantitative. It gives a local assessment of tissue elasticity at each point of interest of an organ. It has been used with success in the evaluation of breast lesions (23).

In an exploratory study, we have assessed the efficiency of SWE in predicting malignancy in solitary or multiple thyroid nodules, and we have compared SWE with conventional US features associated with malignancy.

Patients and Methods

Patients

The study was approved by the French National Committee for the Protection of Patients Participation in Biomedical Research Programs (Comité de Protection des Personnes CCP Sud 1; authorization no. 2006-A00657-44). Each patient and control gave written informed consent before enrollment. The study was conducted during a 10-month period.

Ninety-three patients with thyroid nodules who were referred to the Medical and Surgical Endocrinology Department of Timone University Hospital were included in the study. Sixty-one patients presented with a solitary nodule; 45 were female, age (mean \pm SD) 54 ± 14 (range, 18–78) yr; and 16 were male, age 51.5 ± 12.9 (range, 28–76) yr. Subclinical hypothyroidism was found on two patients, and subclinical hyperthyroidism in one. All others were euthyroid. Thirty-two patients were referred for multiple thyroid nodules (multinodular goiters); 24 were female, age 56.4 ± 12.8 (range, 33–76) yr; and eight were male, age 58 ± 8.1 (range, 47–71) yr. Subclinical hyperthyroidism was found in four patients, and subclinical hypothyroidism in one. Seventy-nine patients underwent surgery: 47 of 61 patients with solitary nodules, and all 32 patients with multinodular thyroid glands. Fourteen of 61 patients in the solitary nodule group with a diagnosis of benign lesion after FNA examination were not operated.

Thirty-nine control patients with normal thyroid function and morphology were explored with US and SWE.

Conventional US and SWE

The system is equipped with all diagnostic US machines and transducers for conventional (B-mode, Harmonic imaging, Spatial Compounding imaging, and Amplitude Doppler) and SWE modes. Conventional US and SWE have been operated with the prototype of the Aixplorer, a new-generation US machine developed by SuperSonic Imagine (Les Jardins de la Duranne, Aix en Provence, France). The SWE was described in detail by Bercoff *et al.* (22). It consists of the generation of a remote radiation force by focused ultrasonic beams, the so-called “pushing beams,” a patented technology called “Sonic Touch.” Several pushing beams at increasing depths are transmitted to generate a quasi-plane shear wave frame that propagates throughout the whole imaging area. After generation of this shear wave, an ultrafast echographic imaging sequence, the Ulmtraast Imaging System, is performed to acquire successive raw radiofrequency dots at a very high frame rate (up to 20,000 frames per second). Based on Young’s modulus formula, the assessment of tissue elasticity can be derived from shear wave propagation speed. A color-coded image is displayed, which shows softer tissue in blue and stiffer tissue in red. Quantitative information is delivered; elasticity index (EI) is expressed in kilo-Pascal (kPa). The clinical evaluation of this technique for breast lesion imaging is under investigation (23). Both steps of SWE are achieved using a linear US probe without requiring any intervention (as pressure) by the operator.

Thyroid function tests

Serum TSH, free T₃, free T₄, and thyroid autoantibodies were measured by chemiluminescent ELECSYS immunoassay.

Histological examination

FNA smears were made using two samples collected from nodules in 14 patients. Conventional cytology, thyroid peroxidase, and dipeptidyl aminopeptidase-4 tests were routinely performed in three slides as previously reported (24). Tissue specimens were obtained after surgery from 79 patients. After fixation, embedding, and staining, tissue sections were examined by two pathologists. Histological typing was based on the World Health Organization criteria.

Statistical analysis

Descriptive statistics were applied to all variables collected. The univariate relation between US characteristics and malignancy was examined by the Fisher exact test for categorized variables. Most clinically and statistically relevant US variables associated with malignancy were incorporated to develop a scoring system. For all analyses, a two-tailed *P* value of less than 0.05 indicated statistical significance. Bootstrap resampling procedures were performed to generate these scoring systems and estimate the confidence intervals (CIs). From the bootstrap samples, we computed a score (Score 1 = US Score). For SWE, the optimal cutoff of EI for diagnosis of malignancy was chosen for a positive predictive value of at least 80%. Another score (Score 2 = US+SWE Score) has been constructed with US and SWE variables. The cutoff levels of both scores were determined for a positive predictive value of at least 80%. Receiver operating characteristic (ROC) curves were performed to estimate the capacity of both scores and SWE alone to predict malignancy using the area under curve (AUC), sensitivity, and specificity, with their 95% CIs. For the score’s analysis, only patients with complete data sets for the parameters were included. All tests were two-sided, and a *P* value <0.05 was considered statistically significant. For analyzing the areas under those correlated ROC curves, a pair-wise comparison of ROC curves for Score 1 (US Score) and Score 2 (US+SWE Score) was performed with a nonparametric approach by using the theory on generalized U-statistics to generate an estimated covariance matrix (25). Analyses were performed with SPSS software (version 15.0; SPSS Inc., Chicago, IL), SPAD version 5.5 and MedCalc 10.4.5.0.

Histology

In 61 patients with solitary nodules, a final diagnosis of malignancy was reported in 15 cases: nine papillary thyroid carcinomas, three follicular carcinomas, one differentiated follicular tumor of uncertain malignant potential (FTUMP), one medullary carcinoma, and one anaplastic carcinoma. In 46 cases, the histology of nodules was benign.

Histology was benign in 24 of 32 patients with multiple thyroid nodules. Fourteen malignant nodules were identified in eight patients: 11 papillary carcinomas, two follicular carcinomas, and one FTUMP. Multifocal malignant nodules were identified in five of eight patients. Sixty-nine benign nodules were recovered in the other 24 patients.

Conventional US patterns

The US features most predictive of malignancy were hypoechogenicity (sensitivity, 70.4%; specificity, 81.8%), absent halo sign (sensitivity, 92.6%; specificity, 41.4%), microcalcifications (sensitivity, 66.7%; specificity, 84.8%), and intranodular vascularity (sensitivity, 51.9%; and specificity, 93.9%). The presence of dense macrocalcifications larger than 2 mm was not predictive of malignancy, with a sensitivity of 22% and a specificity of 79.6%. This type of calcification was detected in 25 nodules by conventional US. Six of the 25 nodules were malignant (Table 1 [1](#)).

TABLE 1. Conventional US patterns and EI in 126 patients (out of 93 patients) with complete data set for all those parameters

	Benign (n = 99)	Cancer (n = 27)	Sensitivity	Specificity
Intranodular vascularity			51.9 (33.1; 70.7)	93.9 (89.2; 98.6)
Present	6	14		
Absent	93	13		
Microcalcifications			66.7 (48.9; 84.5)	84.8 (77.7; 91.9)
Present	15	18		
Absent	84	9		
Macrocalcifications			22.2 (6.5; 37.9)	79.6 (71.7; 87.5)
Present	20	6		
Absent	78	21		
Halo sign			92.6 (82.7; 100)	41.4 (31.7; 51.1)
Absent	58	25		
Present	41	2		
Hypoechogenicity			70.4 (62.4; 78.3)	81.8 (75.1; 88.6)
Present	18	19		
Absent	91	8		
EI			85.2 (71.8; 98.6)	93.9 (89.2; 98.6)
≥65 kPa	6	23		
<65 kPa	93	4		

Data are expressed as number of subjects or percentage (95% CI).

The combination of significant US features (hypoechogenicity, microcalcifications, and intranodular vascularity) increased the specificity of thyroid ultrasonography. These characteristics were used for the construction of Score 1 (US Score) (values between 0 and 100, high values predicting malignancy). Absent halo sign was not included in the final construction of US Score because it did not reach statistical significance with the other parameters. The US Score equation was: 42.18 (if intranodular vascularity = yes) + 6 (if hypoechogenicity = no) + 30.70 (if hypoechogenicity = yes) + 27.13 (if microcalcification = yes). For a positive predictive value of at least 80%, the cutoff level of the US Score for malignancy was defined as 63.6. From the ROC curves, the characteristics of this score to predict a nodule's malignancy were: sensitivity = 51.9% (95% CI = 33.1; 70.7), specificity = 97% (95% CI = 93.6; 100), positive predictive value = 82.4% (95% CI = 64.3; 100), and negative predictive value = 88.1% (95% CI = 82.0; 94.2). The AUC was 84.7 (95% CI = 74.5; 94.9) (*P* < 0.001) (Fig. 1A [1](#)).

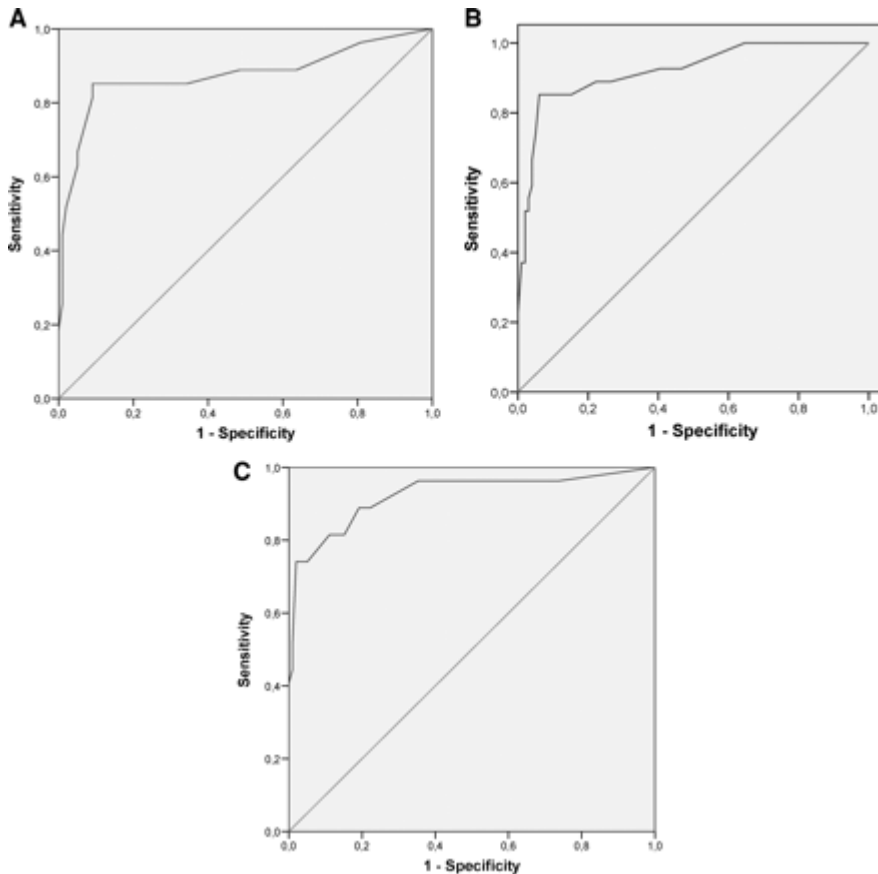


FIG. 1. ROC curves (area under the ROC curve) for changes in scores and nodule's malignancy. A, ROC curve for changes in Score 1 (US Score) (AUC = 84.7%). Area under the ROC curve for changes in Score 1 (US Score) and nodule's malignancy. B, ROC curve for the EI of at least 65 kPa (AUC = 93.6%). Area under the ROC curve for changes in index elasticity and nodule's malignancy. C, ROC curve for the Score 2 (US+SWE Score) (AUC = 93.4%). Area under the ROC curve for changes in Score 2 (US+SWE Score) and nodule's malignancy.

Shear wave elastography

EI was significantly higher in malignant nodules [150 ± 95 (30–356) kPa] than in benign nodules [36 ± 30 (0–200) kPa] and normal thyroid glands [15.9 ± 7.6 (5–35) kPa] ($P < 0.001$). The cutoff level of EI for malignancy was estimated as 65 kPa, for a positive predictive value of at least 80%. With this cutoff value, from the ROC curves, the characteristics of EI to predict malignancy were: sensitivity = 85.2% (95% CI, 71.8; 98.6), specificity = 93.9% (95% CI, 89.2; 98.6), positive predictive value = 80% (95% CI, 65.4; 94.6), negative predictive value = 95.9% (95% CI, 92.0; 99.8), and AUC = 93.6 (95% CI, 86.9; 100) (Fig. 1B). Figure 2 shows the B-mode and SWE images (sagittal views) of a benign nodule (Fig. 2A) and papillary carcinoma (Fig. 2B). In four of 25 malignant nodules (three papillary carcinoma, and one FTUMP), EI was lower than 65 kPa. EI was higher than the cutoff value in all follicular carcinoma and in the single cases of medullary and anaplastic carcinomas (Table 2).

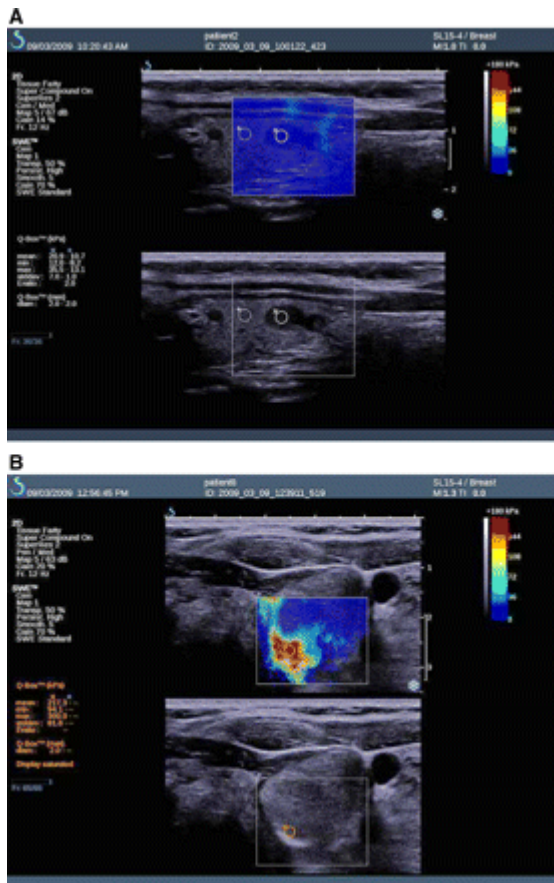


FIG. 2.

Thyroid nodule images obtained on US elastography of a benign thyroid nodule (A) and a papillary carcinoma (B).

TABLE 2. EI of malignant thyroid nodules according to their histological subtypes

Characteristics	n	EI, mean \pm SD (kPa)	Range
Solitary nodules (n = 61)			
Papillary carcinoma	9	148 \pm 98	40-356
Follicular carcinoma	3	117 \pm 72	70-200
Medullary carcinoma	1	263	
Anaplastic carcinoma	1	200	
FTUMP	1	30	
Multiples nodules (n = 83)			
Papillary carcinoma	11	162 \pm 109	30-323
Follicular carcinoma	2	250	
FTUMP	1	180	

The Score 2 = US+SWE score was constructed with US features and EI with the following equation: 39.95 (if intranodular vascularity = yes) + 32.73 (if EI > 65 kPa) + 14.90 (if hypoechogenicity = yes) + 13.42 (if microcalcifications = yes). The cutoff level of US+SWE score for malignancy (for a positive predictive value \geq 80%) was defined as 42.5. From the ROC curves, the characteristics of this score to predict malignancy were: sensitivity = 81.5% (95% CI, 66.9; 96.1), specificity = 97.0% (95% CI, 93.6; 100), positive predictive value = 88% (95% CI, 75.3; 100), negative predictive value = 95.0% (95% CI, 90.7; 99.3), and AUC = 93.4 (95% CI, 86.4; 100) (Fig. 1C). The US characteristics and US+SWE scores of malignant nodules with an EI lower than 65 kPa suggest that two of four nodules are indeed malignant (Table 3). In 25 nodules, macrocalcifications were detected by US. Six of 25 nodules were malignant, and EI was higher than 65 kPa in five of six. Nineteen of 25 nodules were benign, and EI was higher than 65 kPa in five of 19.

TABLE 3.

Echographic characteristics in patients with malignant nodules and EI < 65 kPa

Patient ID	Histology	Hypoechoogenicity	Microcalcification	Central vascularity	No halo sign	EI (kPa)
A1	Papillary (foll. variant)	0	0	0	+	50
A6	Papillary (foll. variant)	+	+	+	0	30
B36	Papillary	+	+	+	+	40
B27	FTUMP	+	0	0	0	30

Foll. variant, Follicular variant of papillary carcinoma; 0, absent; +, present.

Discussion

In our experience, SWE was a powerful tool for the diagnosis of malignancy in thyroid nodules. EI was significantly higher in malignant than benign nodules. Using a cutoff level of 65 kPa, the sensitivity and specificity of the technique were 85.2 and 93.9%, respectively. These data are in agreement with previous reports based on other methods of elastography. Indeed, in three studies using real-time elastography with off-line processing of strain images, the sensitivity ranged between 82 and 88%, and the specificity between 81.8 and 96% ([11](#), [12](#), [13](#)). With a commercial US apparatus using a freehand compression applied on the neck region and a real-time measurement on a numerical scale, the sensitivity and specificity were estimated between 94 and 100% and between 81 and 100%, respectively ([14](#), [15](#), [16](#)).

SWE is operator-independent and more reproducible than static elastography. It offers other advantages. First, it is quantitative. Second, it provides local elasticity estimation of nodules that is unaltered by the presence of a hard area in the vicinity. This is of major interest in cases of multinodular thyroid. This group of patients may represent up to 40% of all patients referred for thyroid nodules ([18](#)). As indicated previously, the risk of cancer per patient in this group has been appreciated either lower ([19](#), [20](#)) or equal ([21](#)) to that in solitary nodules. Most cases of multinodular goiters are not suitable for static elastography because the nodule to be examined with this technique must be clearly distinguishable from other nodules in the thyroid gland ([7](#), [26](#)).

The accuracy of EI measurement may also be altered if nodules are close to the carotid artery because arterial pulsation may create elastographic images and therefore alter the adequate acquisition and accurate interpretation of the data. In nodules with a diameter greater than 3 cm, adequate compression of the whole nodule may not be obtained. Similarly, elastography using external compression was considered unreliable in nodules with calcified shells or rims because the US beam does not cross these macrocalcifications, and no tissue strain is obtained by the probe pressure ([14](#), [26](#)). In these cases, SWE may offer some advantages over this technique. In our study, 19 of 25 thyroid nodules with macrocalcifications were benign, and SWE measurement was valid in 14 cases. Although SWE may be used in the presence of macrocalcifications, one must be cautious in the interpretation of SWE. In previous literature, coarse or rim macrocalcifications have been documented as having no diagnostic value for cancer ([27](#), [28](#)), although they have been shown to double the risk of malignancy in one recent study ([21](#)). The association of nodule macrocalcifications with an EI higher than 65 kPa may indicate surgery, although the false-positive rate for benign nodules may reach 26% as shown in our study.

Other US elastography techniques are time consuming and not routinely useful. The US elastography using generation of tissue movement by carotid artery is still limited to the research area because it needs a long time after processing for calculation of the thyroid nodule stiffness ([17](#)). The first technique of real-time elastography and off-line processing of strain images is also time-consuming because analysis after data acquisition takes over 30 min ([11](#), [12](#), [13](#)). Thyroid nodule SWE updates elasticity information in real time, and this information is directly interpreted by the radiologist in a straightforward manner, as in the traditional workflow of standard US.

The subtype of thyroid nodules may be the source of variations in EI. Indeed, in the evaluation of breast lesions, a good relationship was found between elasticity score and histology ([23](#), [28](#)).

Papillary carcinoma is the most frequent subtype of malignant thyroid nodules. Increased cellularity and cellular compaction, the main characteristics of papillary carcinoma, are the histological basis for hypoechogenicity and stiffness. As indicated above, EI was significantly higher in papillary carcinoma than in benign nodules. However, follicular and other histological variants of papillary carcinoma are possible. In our study, EI in malignant nodules ranges from 30 to 356 kPa, with four of 20 malignant nodules with EI less than 65 kPa, not significantly different from those of benign thyroid nodules. The combination of several conventional US features highly suggestive of papillary carcinoma has been found in two of four cases. In the two other cases, a 9.2-mm papillary carcinoma and a FTUMP, none of these conventional US features have been found (Table 31). In contrast, follicular carcinomas are composed of small microfollicles with variable amounts of colloid. Therefore, their echogenicity and EI may depend on their cellular content. Conventional US is not predictive in follicular lesions (29), although irregular halo and iso- or hyperechogenicity have been described in follicular thyroid cancer (30). In our study, EI ranges from 70 to 250 kPa with a possible correlation with stroma content that will need further study. Similar data have been obtained by Rago *et al.* (14). However, elastography was not efficient for diagnosis of follicular carcinoma in two other studies (13, 15). More studies in correlation with various histological criteria will be helpful in understanding this discrepancy. Two cases of FTUMP are present in our series. In one case, EI was 30 kPa, and in the other case EI was 180 kPa.

The place of SWE in the evaluation of thyroid nodules for potential malignancy needs to be established. Actually, this evaluation is based upon clinical examination, conventional US characteristics, and FNA above all. Despite its benefits, FNA is limited by sampling and cytological diagnostic difficulties. US-guided FNA (31), more detailed classification of inconclusive aspirates (18), as well as multidisciplinary and institutional efforts for the evaluation of thyroid nodules (18) have significantly improved the diagnosis of thyroid cancer. In our study, a cutoff value of 65 kPa alone provided a positive predictive value of 92.3%, suggesting that SWE might be considered as a first-line imaging technique for thyroid nodules because it provides a sensitivity of 85.2% and a specificity of 93.9%. On the basis of EI determination with a cutoff value of 65 kPa, four cases of malignant nodules, including one FTUMP, would have been missed. The 13.8% rate of false-negative tests is not acceptable. Further evaluation of these nodules by an expert radiologist reduces false-negative results to two cases previously detailed. On the other hand, EI was higher than 65 kPa in 6.1% of benign nodules. This rate could be considered acceptable because FNA and possibly thyroid surgery are indicated for this condition. Indeed, the sensitivity of the combination of several conventional US characteristics is much lower (51.9%). Therefore, almost 50% of the malignant nodules would have been missed. The specificity is high (97%), when thyroid US is performed by experienced radiologists. The construction of the US+SWE score with the combination of EI and US characteristics associated with cancer gives a sensitivity of 81.5% and a specificity of 97%. On the basis of this score, about 18% of the malignant nodules would have been missed.

The lower sensitivity of US characteristics, alone or in association with EI, leads us to support SWE as the first-line procedure in the evaluation of thyroid nodules. When EI is at least 65 kPa, further exploration is needed by FNA or thyroid surgery. For nodules with an EI of less than 65 kPa, careful evaluation of US signs associated with cancer may add useful information for the management of patients. Indeed, in our study, US signs suggestive of carcinoma were found in two of four cases with EI of less than 65 kPa. The successive use of SWE and US characterization was effective, except in a 9.2-mm papillary carcinoma and one FTUMP. Further studies are needed to test whether thyroid SWE has the potential to reduce the number of FNA biopsies by detecting benign thyroid nodules using an EI cutoff value.

In conclusion, promising results have been obtained with SWE in the evaluation of thyroid nodules. This newly developed technique may be applied to multinodular goiters. It seemed easy to apply. Larger prospective studies are needed to confirm our results, define the respective place of SWE vs. US and FNA, and test the diagnostic accuracy of our algorithm.

Footnotes

The CERIMED project is funded by the French Ministry of Education and Research, The City Hall of Marseilles, the Departmental and Regional Councils, and the European Regional Development Fund. It has also been supported by a grant from the French Cancer National Institute. This research was supported by a grant from the Assistance Publique des Hôpitaux de Marseille (Clinical Research Call, 2006). Disclosure Summary: The authors have nothing to disclose. **First Published Online September 29, 2010**

Abbreviations: AUC, Area under curve; CI, confidence interval; EI, elasticity index; FNA, fine-needle aspiration; FTUMP, follicular tumor of uncertain malignant potential; kPa, kilo-Pascal; ROC, receiver operating characteristic; SWE, shear wave elastography; US, ultrasound.

References

1. [↓](#)
Tunbridge WM, Evered DC, Hall R, Appleton D, Brewis M, Clark F, Evans JG, Young E, Bird T, Smith PA 1977 The spectrum of thyroid disease in a community: the Whickham survey. *Clin Endocrinol (Oxf)* 7:481–493 [Medline](#)
2. [↓](#)
Guth S, Theune U, Aberle J, Galach A, Bamberger CM 2009 Very high prevalence of thyroid nodules detected by high frequency (13 MHz) ultrasound examination. *Eur J Clin Invest* 39:699–706 [CrossRefMedline](#)
3. [↓](#)
Hegedüs L, Bonnema SJ, Bennedbaek FN 2003 Management of simple nodular goiter: current status and future perspectives. *Endocr Rev* 24:102–132 [Abstract/FREE Full Text](#)
4. [↓](#)
Frates MC, Benson CB, Charboneau JW, Cibas ES, Clark OH, Coleman BG, Cronan JJ, Doubilet PM, Evans DB, Goellner JR, Hay ID, Hertzberg BS, Intenzo CM, Jeffrey RB, Langer JE, Larsen PR, Mandel SJ, Middleton WD, Reading CC, Sherman SI, Tessler FN 2005 Management of thyroid nodules detected at US: Society of Radiologists in Ultrasound consensus conference statement. *Radiology* 237:794–800 [Abstract/FREE Full Text](#)
5. [↓](#)
Nam-Goong IS, Kim HY, Gong G, Lee HK, Hong SJ, Kim WB, Shong YK 2004 Ultrasonography-guided fine-needle aspiration of thyroid incidentaloma: correlation with pathological findings. *Clin Endocrinol (Oxf)* 60:21–28 [CrossRefMedline](#)
6. [↓](#)
Gharib H, Goellner JR 1993 Fine-needle aspiration biopsy of the thyroid: an appraisal. *Ann Intern Med* 118:282–289 [Abstract/FREE Full Text](#)
7. [↓](#)
Alexander EK 2008 Approach to the patient with a cytologically indeterminate thyroid nodule. *J Clin Endocrinol Metab* 93:4175–4182 [Abstract/FREE Full Text](#)
8. [↓](#)
Cáp J, Ryska A, Rehorková P, Hovorková E, Kerekes Z, Pohnetalová D 1999 Sensitivity and specificity of the fine needle aspiration biopsy of the thyroid: clinical point of view. *Clin Endocrinol (Oxf)* 51:509–515 [CrossRefMedline](#)
9. [↓](#)
Raab SS, Vrbín CM, Grzybicki DM, Sudilovsky D, Balassanian R, Zarbo RJ, Meier FA 2006 Errors in thyroid gland fine-needle aspiration. *Am J Clin Pathol* 125:873–882 [Abstract/FREE Full Text](#)
10. [↓](#)
Ophir J, Céspedes I, Ponnekanti H, Yazdi Y, Li X 1991 Elastography: a quantitative method for imaging the elasticity of biological tissues. *Ultrason Imaging* 13:111–134 [CrossRefMedline](#)
11. [↓](#)
Lyshchik A, Higashi T, Asato R, Tanaka S, Ito J, Mai JJ, Pellot-Barakat C, Insana MF, Brill AB, Saga T, Hiraoka M, Togashi K 2005 Thyroid gland tumor diagnosis at US elastography. *Radiology* 237:202–211 [Abstract/FREE Full Text](#)
12. [↓](#)
Rubaltelli L, Corradin S, Dorigo A, Stabilito M, Tregnaghi A, Borsato S, Stramare R 2009 Differential diagnosis of benign and malignant thyroid nodules at elastosonography. *Ultraschall Med* 30:175–179 [CrossRefMedline](#)
13. [↓](#)
Hong Y, Liu X, Li Z, Zhang X, Chen M, Luo Z 2009 Real-time ultrasound elastography in the differential diagnosis of benign and malignant thyroid nodules. *J Ultrasound Med* 28:861–867 [Abstract/FREE Full Text](#)

14. [↓](#)
Rago T, Santini F, Scutari M, Pinchera A, Vitti P 2007 Elastography: new developments in ultrasound for predicting malignancy in thyroid nodules. *J Clin Endocrinol Metab* 92:2917–2922 [Abstract/FREE Full Text](#)
15. [↓](#)
Asteria C, Giovanardi A, Pizzocaro A, Cozzaglio L, Morabito A, Somalvico F, Zoppo A 2008 US-elastography in the differential diagnosis of benign and malignant thyroid nodules. *Thyroid* 18:523–531 [CrossRefMedline](#)
16. [↓](#)
Tranquart F, Bleuzen A, Pierre-Renoult P, Chabrolle C, Sam Giao M, Lecomte P 2008 [Elastosonography of thyroid lesions]. *J Radiol* 89:35–39 [CrossRefMedline](#)
17. [↓](#)
Dighe M, Bae U, Richardson ML, Dubinsky TJ, Minoshima S, Kim Y 2008 Differential diagnosis of thyroid nodules with US elastography using carotid artery pulsation. *Radiology* 248:662–669 [Abstract/FREE Full Text](#)
18. [↓](#)
Yassa L, Cibas ES, Benson CB, Frates MC, Doubilet PM, Gawande AA, Moore Jr FD, Kim BW, Nosé V, Marqusee E, Larsen PR, Alexander EK 2007 Long-term assessment of a multidisciplinary approach to thyroid nodule diagnostic evaluation. *Cancer* 111:508–516 [CrossRefMedline](#)
19. [↓](#)
Boelaert K, Horacek J, Holder RL, Watkinson JC, Sheppard MC, Franklyn JA 2006 Serum thyrotropin concentration as a novel predictor of malignancy in thyroid nodules investigated by fine-needle aspiration. *J Clin Endocrinol Metab* 91:4295–4301 [Abstract/FREE Full Text](#)
20. [↓](#)
Rago T, Fiore E, Scutari M, Santini F, Di Coscio G, Romani R, Piaggi P, Ugolini C, Basolo F, Miccoli P, Pinchera A, Vitti P 2010 Male sex, single nodularity, and young age are associated with the risk of finding a papillary thyroid cancer on fine-needle aspiration cytology in a large series of patients with nodular thyroid disease. *Eur J Endocrinol* 162:763–770 [Abstract/FREE Full Text](#)
21. [↓](#)
Frates MC, Benson CB, Doubilet PM, Kunreuther E, Contreras M, Cibas ES, Orcutt J, Moore Jr FD, Larsen PR, Marqusee E, Alexander EK 2006 Prevalence and distribution of carcinoma in patients with solitary and multiple thyroid nodules on sonography. *J Clin Endocrinol Metab* 91:3411–3417 [Abstract/FREE Full Text](#)
22. [↓](#)
Bercoff J, Tanter M, Fink M 2004 Supersonic shear imaging: a new technique for soft tissue elasticity mapping. *IEEE Trans Ultrason Ferroelectr Freq Control* 51:396–409 [CrossRefMedline](#)
23. [↓](#)
Tanter M, Bercoff J, Athanasiou A, Deffieux T, Gennisson JL, Montaldo G, Muller M, Tardivon A, Fink M 2008 Quantitative assessment of breast lesion viscoelasticity: initial clinical results using supersonic shear imaging. *Ultrasound Med Biol* 34:1373–1386 [CrossRefMedline](#)
24. [↓](#)
De Micco C, Zoro P, Garcia S, Skoog L, Tani EM, Carayon P, Henry JF 1994 Thyroid peroxidase immunodetection as a tool to assist diagnosis of thyroid nodules on fine-needle aspiration biopsy. *Eur J Endocrinol* 131:474–479 [Abstract/FREE Full Text](#)
25. [↓](#)
DeLong ER, DeLong DM, Clarke-Pearson DL 1988 Comparing the areas under two or more correlated receiver operating characteristic curves: a nonparametric approach. *Biometrics* 44:837–845 [CrossRefMedline](#)
26. [↓](#)
Rago T, Vitti P 2008 Role of thyroid ultrasound in the diagnostic evaluation of thyroid nodules. *Best Pract Res Clin Endocrinol Metab* 22:913–928 [CrossRefMedline](#)
27. [↓](#)

- Kim EK, Park CS, Chung WY, Oh KK, Kim DI, Lee JT, Yoo HS** 2002 New sonographic criteria for recommending fine-needle aspiration biopsy of nonpalpable solid nodules of the thyroid. *AJR Am J Roentgenol* 178:687–691 [Abstract/FREE Full Text](#)
28. [↓](#)
Tan SM, Teh HS, Mancer JF, Poh WT 2008 Improving B mode ultrasound evaluation of breast lesions with real-time ultrasound elastography—a clinical approach. *Breast* 17:252–257 [CrossRefMedline](#)
29. [↓](#)
Rago T, Di Coscio G, Basolo F, Scutari M, Elisei R, Berti P, Miccoli P, Romani R, Faviana P, Pinchera A, Vitti P 2007 Combined clinical, thyroid ultrasound and cytological features help to predict thyroid malignancy in follicular and Hupsilonrthle cell thyroid lesions: results from a series of 505 consecutive patients. *Clin Endocrinol (Oxf)* 66:13–20 [Medline](#)
30. [↓](#)
Jeh SK, Jung SL, Kim BS, Lee YS 2007 Evaluating the degree of conformity of papillary carcinoma and follicular carcinoma to the reported ultrasonographic findings of malignant thyroid tumor. *Korean J Radiol* 8:192–197 [CrossRefMedline](#)
31. [↓](#)
Morris LF, Ragavendra N, Yeh MW 2008 Evidence-based assessment of the role of ultrasonography in the management of benign thyroid nodules. *World J Surg* 32:1253–1263 [CrossRefMedline](#)

Foram estudados também 15 casos de patologia prostática pelo Dr. J M Correias de Paris e os resultados preliminares indicam que a hiperplasia prostática benigna = 29 ± 19 kPA e o CA próstata 65 ± 56 kPA. Esses resultados são bem melhores do que o US convencional com Doppler ou contraste da próstata .

Também foi realizado uma comparação entre o FIBROSCAN e a tecnologia ARFI do AS 2000 e o FIBROSCAN falhou em 12.5% dos casos e em nenhum dos casos da tecnologia ARFI.

[J Gastroenterol](#). 2012 Jan 6. [Epub ahead of print]

Head-to-head comparison of transient elastography (TE), real-time tissue elastography (RTE), and acoustic radiation force impulse (ARFI) imaging in the diagnosis of liver fibrosis.

[Colombo S](#), [Buonocore M](#), [Del Poggio A](#), [Jamoletti C](#), [Elia S](#), [Mattiello M](#), [Zabbialini D](#), [Del Poggio P](#).

Source **Hepatology Unit, Treviglio Hospital, Piazza Ospedale n.1, 24047, Treviglio (Bergamo), Italy.**

Abstract

BACKGROUND:

Real-time tissue elastography (RTE), acoustic radiation force impulse (ARFI) imaging, and transient elastography (TE) are new technologies that are used for liver stiffness evaluation. The aim of this study was to compare these methods in the same population and to determine their diagnostic accuracy in the prediction of liver fibrosis.

METHODS:Forty-five consecutive, previously biopsied, patients with chronic liver disease and 27 normal subjects underwent TE, RTE, and ARFI on the right liver lobe. Correlation coefficients between measurements, Metavir fibrosis stage, and histological necro-inflammatory activity (adjusted for fibrosis stage) were evaluated via Spearman's rank order correlation coefficients. Areas under the receiver operating characteristic curve (AUROCs) were calculated to predict each fibrosis stage.

RESULTS: Failure or inconsistent results occurred in 12.5% of the attempts at TE, but in none of the attempts at RTE and ARFI. The three methods showed high correlation with fibrosis and poor correlation with necro-inflammatory activity. TE and ARFI exhibited high diagnostic accuracy (AUROCs ≥ 0.9) in diagnosing cirrhosis (F4 Metavir). All three methods presented fair (AUROCs >0.7) to good (AUROCs >0.8) diagnostic accuracy in diagnosing fibrosis (F1-4 Metavir) and significant fibrosis (F2-4 Metavir), with TE showing the best performance (AUROCs were 0.878 for fibrosis and 0.897 for significant fibrosis).

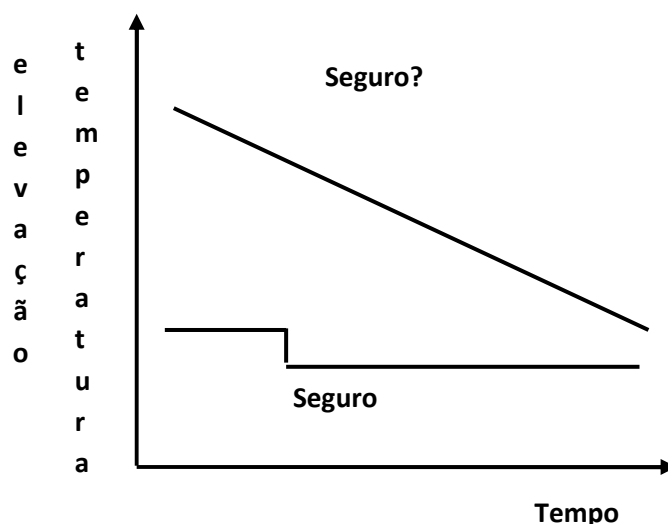
CONCLUSIONS: TE and ARFI provide high diagnostic accuracy in the diagnosis of cirrhosis. When feasible, TE may perform better than RTE and ARFI in predicting fibrosis and significant fibrosis, but larger studies are needed.

Conclusão: a elastografia que utilize as ondas de cisalhamento é um campo em maturação e que permite grandes possibilidades de aplicações médicas.

A última parte dessa sessão que abordou as imagens decorrentes da ondas de cisalhamento foi ministrada pelo Dr. Keith Wear, Phd que falou sobre **Safety and Effectiveness Evaluation Issues for shear wave Imaging Using, Acoustic Radiation Force** e é membro da Saúde Radiológica do FDA, Silver Spring Maryland USA

As preocupações quanto a segurança da **força de irradiação acústica**, da qual é formada as imagens de velocidades da ondas de cisalhamento, decorrem dos seguintes pontos principais :

1. **Efeito térmico** que é a medida do potencial para aumento da temperatura no tecido, em decorrência de uma série rápida e repetida de pulsos acústicos de curta duração, para os quais a intensidade temporal média é relevante. Entretanto, a força de irradiação acústica, da qual é formada as imagens de velocidades das ondas de cisalhamento, tem uma intensidade temporal média baixa e também frequentemente utiliza séries com baixa taxa de repetição de pulsos acústicos de alta intensidade e alta duração.



Palmere detectou que a elevação típica de temperatura na ARFI = 6°C

Dahh detectou que o aumento da temperatura pode ser mitigado por diferentes tipos de processamento do sinal.

2. Existe uma preocupação quanto ao aumento da temperatura que possa ocorrer em vivo durante a emissão dos pulsos, especialmente quando um **tecido de elevada absorção** é examinado, tal como o osso.
3. Algumas publicações recentes relataram **potência acústica emitida (MI) pela força de irradiação acústica**, da qual é formada as imagens de velocidade de propagação das ondas de cisalhamento, acima dos limites permitidos pelo FDA. O MI foi formulado presumindo-se a duração do pulso = 1 ciclo. O limite para produzir cavitação diminui à medida que a duração do pulso se estende além de uns poucos ciclos. Os pulsos ARFI in vivo podem utilizar até 200 pulsos. A movimentação do paciente pode intervir na aquisição das imagens que utilizam as ondas de cisalhamento.
4. Também existem preocupações quanto a **efetividade das medidas das velocidades da onda de cisalhamento** força de irradiação acústicas estimarem corretamente a elasticidade dos tecidos. A forma utilizada estabelece presunções que podem não ser totalmente satisfatória para tecidos humanos vivos.
5. As medidas das **velocidades das ondas de cisalhamento** podem variar com fatores tais como:
 - **freqüência do US e propriedades dos feixes dos transdutores;**
 - A velocidade das ondas de cisalhamento dependem da freqüência da sonda e da **dispersão do feixe;**
 - A velocidade também depende da **profundidade do local mensurado** na mama, no fígado e nos phatons;
 - A dureza do fígado aumenta a medida que aumenta a **pressão venosa** no parênquima hepático;
 - A velocidade pode depender da **pressão sanguínea**
 - A velocidade pode ser influenciada pelas **ondas refletidas**
 - A velocidade pode ser influenciada pela s **atividades cardíaca, respiratória e circulatória;**
 - A velocidade pode ser influenciada pelo **operador, etc.**

Se esses fatores não são levados em conta adequadamente eles poderão produzir variabilidades que podem degradar o valor do diagnóstico e as medidas das **velocidades das ondas de cisalhamento** devem aguardar sua consolidação. A menção de produtos comerciais, suas fontes ou seu uso em conexão com o material relatado aqui não é para ser relatado com o aval do FDA, real ou implícito.

